CrossMark

ORIGINAL PAPER

A glassy carbon electrode modified with porous Cu₂O nanospheres on reduced graphene oxide support for simultaneous sensing of uric acid and dopamine with high selectivity over ascorbic acid

**Li-Ping Mei[1] · Jiu-Ju Feng[1] · Liang Wu[1] · Jian-Rong Chen[1] · Liguo Shen[1] ·
Yunlong Xie[1,2] · Ai-Jun Wang[1]**

Abstract Porous cuprous oxide nanospheres were deposited on reduced graphene oxide (pCu₂O NS-rGO) by a solvothermal approach that uses hexadecyltrimethylammonium bromide as the capping agent and L-glutamic acid as the reducing agent. The nanomaterial was characterized by transmission electron microscopy, Raman spectroscopy, thermogravimetry, and electrochemical methods. A glassy carbon electrode was modified with pCu₂O NS-rGO, and the respective electrode displays a well expressed oxidation peak for dopamine (DA) located at 160 mV (vs. SCE). It also gives a strong peak for uric acid (UA) which is separated from the DA peak by 130 mV (vs. SCE). No signals can be detected for ascorbic acid (AA) in concentrations up to 2.0 mM. The findings are exploited in a method for simultaneous determination of UA and DA. The linear ranges are from 1.0 to 138 μM for UA, and from 0.05 to 109 μM for DA even in the presence of relatively high concentrations of AA. The detection limits are 112 nM for UA and 15 nM for DA (at an S/N ratio of 3).

Introduction

Dopamine (DA) is a neurotransmitter in hypothalamus and pituitary gland, which has direct effects on human emotion [1, 2]. Low concentration of DA can induce several diseases including Schizophrenia and Parkinson's disease [3]. Similarly, uric acid (UA) is widely investigated as the main final product of purine metabolism [4]. Abnormalities of UA levels in biological fluid will cause several diseases such as gout and hyperuricemia [5]. UA and DA as electroactive molecules can be measured by electrochemical methods [6], which have the advantages of convenience, rapidity, and high sensitivity over the other methods [7].

Nonetheless, ascorbic acid (AA) usually coexists with UA and DA in human blood and/or urine [8], and their electrochemical signals cannot be separated on conventional bare electrode because of their overlapped oxidation peaks [9]. Hence, it is greatly imperative to exploit a highly selective and sensitive electrochemical approach for simultaneous testing of UA and DA containing AA.

Numerous materials such as ion-exchange membrane [3, 10], conducting polymer [11], carbon-based nanomaterials [12], metal and metal oxide [13, 14] have been used to improve the electrochemical responses of these biomolecules. Among them, cuprous oxide (Cu₂O), a p-type semiconductor, is an attractive electrode material [15]. Cu₂O has wide applications in CO oxidation [16], catalysis [17], and biosensing [18], due to its low band-gap energy (2.17 eV), high catalytic activity, superior conductivity, and relatively low price. Up to

✉ Yunlong Xie
   xieyunlong@zjnu.edu.cn

✉ Ai-Jun Wang
   ajwang@zjnu.cn

1   College of Geography and Environmental Science, College of Chemistry and Life Science, Zhejiang Normal University, Jinhua 321004, China

2   Xingzhi College, Zhejiang Normal University, Jinhua 321004, China

now, there are a variety of Cu_2O nanomaterials with different morphologies such as rods [19], wires [20], porous spheres [21], and cubes [22]. Particularly, porous Cu_2O nanospheres are considered as promising electrode materials for determination of some electroactive species, because of their high surface area and more active sites accessible [23, 24].

Graphene and its derivates attract tremendous attention in electrochemical sensors [25], owing to their enhanced electrical conductivity and enlarged electroactive surface area. For example, Li's group fabricated reduced graphene sheet films for the determination of β-nicotinamide adenine dinucleotide [26]. In another example, Xu et al. synthesized Pt/rGO for concurrent detection of UA and DA in the presence of of AA [27].

Herein, porous Cu_2O nanospheres supported on rGO (pCu$_2$O NS-rGO) were synthesized by a one-pot solvothermal approach, using L-glutamic acid and hexadecyltrimethylammonium bromide (CTAB) as the reducing agent and structure-directing agent, respectively. The nanocomposites were extended for constructing a sensor to simultaneously detect UA and DA in the presence of AA.

Experimental section

Chemicals

Graphite powder (99.95 %, 8000 mesh), copper(II) nitrate trihydrate ($Cu(NO_3)_2 \cdot 3H_2O$), L-glutamic acid, hexadecyltrimethylammonium bromide (CTAB), ascorbic acid (AA), dopamine (DA), uric acid (UA), acetaminophen, citric acid, glycine, lysine, fructose, and glucose were supplied by Shanghai Aladdin Chemical Reagent Company (Shanghai, China, www.chemicalbook.com) with the analytical grade. All the chemicals were used as received.

Preparation of pCu$_2$O NS-rGO

Typically, a modified Hummers' method was applied to prepare graphene oxide (GO), as reported in our previous work [28]. In brief, 1.0 g of natural graphite powder, 1.0 g of $NaNO_3$ and 33 mL of 98 % H_2SO_4 were put into a 250 mL beaker, successively. Then, 6.0 g of $KMnO_4$ was slowly added into the mixed solution under stirring at 0 °C. The ice-bath was removed and the mixture was heated at 35 °C for 1.5 h. Subsequently, 40 mL of water was slowly added into the system under stirring. Afterwards, the temperature was up to 95 °C for 30 min. Next, another 100 mL of water and 6 mL of 30 % H_2O_2 was added into the above mixture. The color of the reaction system was changed from blackish brown to earthy yellow. Finally, the resultant mixture was cooled to room temperature and centrifuged at 1000 rpm for 5 min. Then, the solution was placed over one night and washed by centrifuging at 4000 rpm for 5 min until the pH value of the upper layer of the suspension arrived at near 7. A homogeneous suspension is obtained after filtering the trace residues.

For the preparation of pCu$_2$O NS-rGO, 0.5 g of CTAB and 5 mL of GO (1.0 mg mL^{-1}) were dispersed into 15 mL of ethanol by stirring. 0.121 g of $Cu(NO_3)_2 \cdot 3H_2O$, and 0.3 g of

Fig. 1 a, b TEM and c HRTEM images of pCu$_2$O NS-rGO. d Nitrogen adsorption/desorption analysis of pCu$_2$O NS-rGO. Insets in B and D show the corresponding SAED pattern and pore-size distribution, respectively.
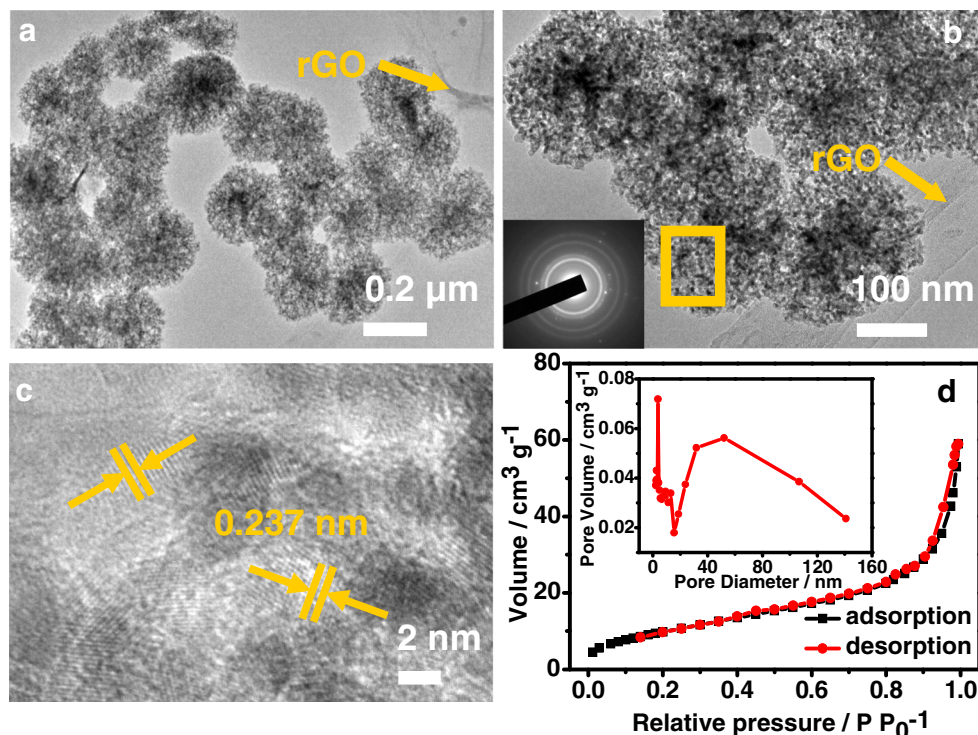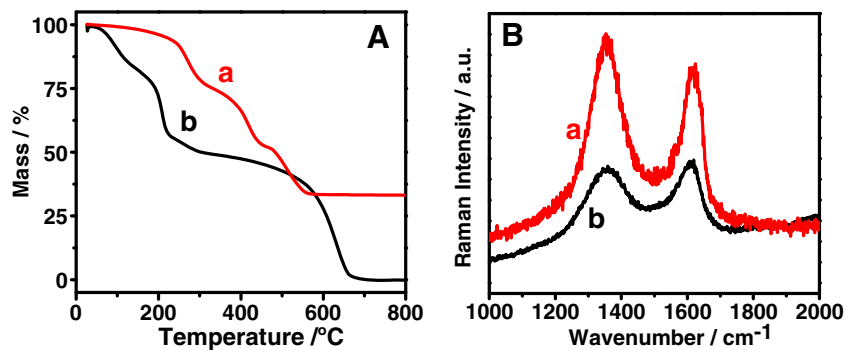
L-glutamic acid were added into the above solution subsequently. After stirring for 30 min, the mixture was transferred into a 25 mL Teflon-lined stainless-steel autoclave and heated at 160 °C for 6 h. After cooling to room temperature, the products were separated via centrifugation and thoroughly washed using ethanol and water. Finally, the purified samples were dried in vacuum at 60 °C for further use.

In control experiments, Cu$_2$O nanoparticles (NPs) were prepared without CTAB in the identical procedure. Pure rGO was obtained by reducing GO with freshly prepared NaBH$_4$ solution (0.5 M).

Characterization

Transmission electron microscopy (TEM) and high-resolution transmission electron microscopy (HRTEM) measurements (www.jeol.co.jp/en.com) were carried out on a JEM-2100F transmission electron microscope equipped with the selective area electron diffraction (SAED). The crystalline nature was examined by X-ray diffraction (XRD, Rigaku Dmax-2000 diffractometer, www.rigaku.com) with Cu-Kα radiation (Bruker Co., Germany). X-ray photoelectron spectra (XPS, www.pharmaceuticalonline.com) were recorded on a Thermo SCIENTIFIC ESCALAB 250 XPS spectrometer with Al Kα X-ray radiation (1486.6 eV). Raman spectra were acquired on a micro-Raman system (Renishaw RM1000 spectrometer) with an excitation wavelength of 633 nm (www.antpedia.com). Thermogravimetric analysis (TGA) was conducted with a simultaneous thermo-gravimetric analyzer (NETZSCH STA 449C, www.brain-power.com). The samples were heated in air from room temperature to 800 °C at a heating rate of 10 °C min^{-1}.
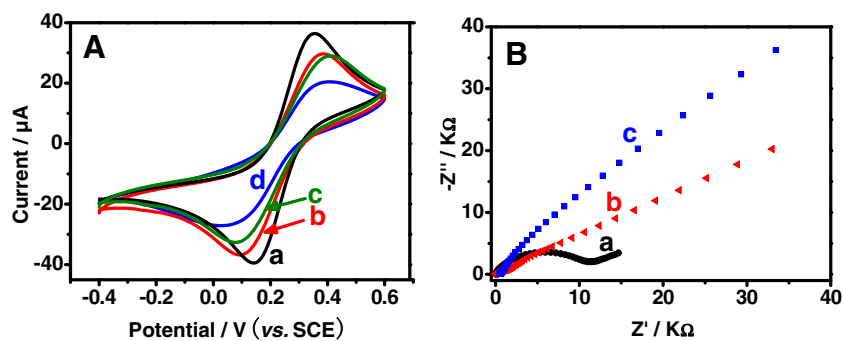
Electrochemical measurements

All the electrochemical measurements were conducted on a CHI 660D electrochemical workstation (Chenhua Instruments Co., Shanghai, China, www.chinstruments.com), and performed on a conventional three-electrode system, which includes a bare or modified glass carbon electrode (GCE, 3.
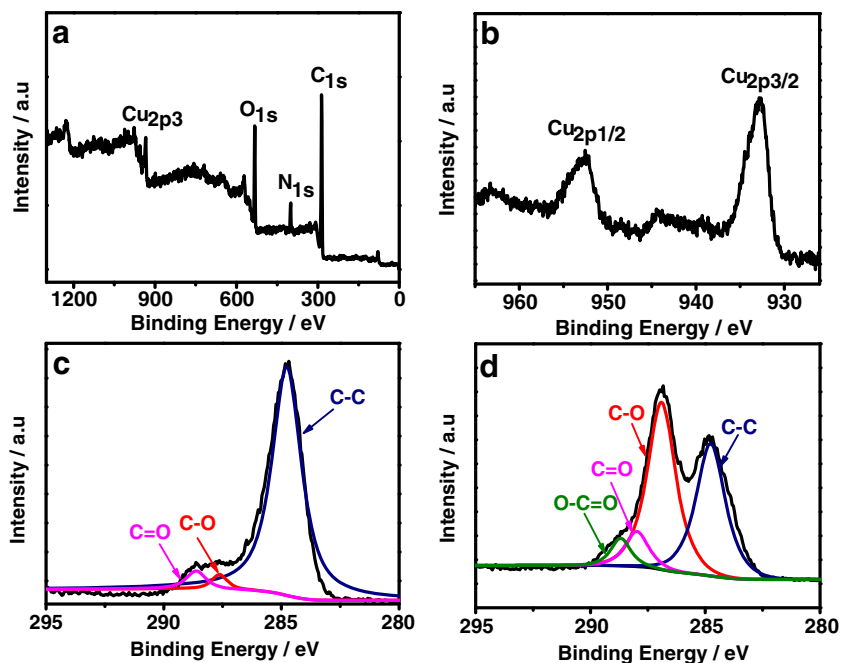
0 mm in diameter) as the working electrode, a platinum wire as the counter electrode, and a saturated calomel electrode (SCE) as the reference electrode. All the electrochemical experiments were carried out at room temperature, if not stated otherwise.

For the construction of pCu$_2$O NS-rGO modified electrode (pCu$_2$O NS-rGO/GCE), the sample was diluted to 1.0 mg mL^{-1} with water and sonicated for 30 min to form a homogenous dispersion. Then, 6 μL of the dispersion was transferred onto the electrode surface. After drying in air, Nafion (0.05 %) with the volume of 5 μL was coated on the surface of the catalyst. For comparison, Cu$_2$O NPs and rGO modified electrodes were constructed under the identical conditions, named as Cu$_2$O NPs/GCE and rGO/GCE, respectively.

Differential pulse voltammetry (DPV) measurements were performed to estimate the electrocatalytic activity of the catalyst toward UA and/or DA oxidation in the presence of 2.0 mM AA in 0.1 M phosphate buffer (pH 7.0) at a sweep rate of 50 mV s^{-1}.

Results and discussion

Characterization

Low- and high-resolution transmission electron microscopy (TEM) images were provided to illustrate the detailed structural information of the typical product (Fig.1a and b). The sample was composed of many uniformly dispersed spherical particles with the mean diameter of 223 ± 8 nm on the surface of rGO with well-resolved fringes as marked by the arrows. The polycrystalline property of the resultant Cu$_2$O nanospheres was demonstrated by the selected area electron diffraction pattern, as seen in inset of Fig. 1b.

As observed in Fig. 1c, the distinguished lattice fringes with the measured d-spacing distance of 0.24 nm were obtained, which is matched well with the (111) crystal planes of Cu$_2$O [29]. This observation is similar to Cu$_2$O nanocrystals in the literature [30]. Moreover, the porous structure of Cu$_2$O nanospheres is clearly observed, which is assembled by many small primary particles.

Nitrogen adsorption-desorption isotherms were carried out at 77.4 K to further testify the porosity of Cu$_2$O nanospheres (Fig. 1d). The isotherms exhibit type V hysteresis loops with a large hysteresis loop, providing the strong evidence for the formation of porous structures. The BET surface area and pore volume are calculated to be 38.04 ± 0.05 cm^2 g^{-1} and 0.077 ± 0.002 cm^3 g^{-1}, respectively. The enlarged surface area and pore volume strongly demonstrate the formation of porous structure. It is believed that a high surface area favors the efficient contact between active materials and reactants in the electrolyte, thereby providing more electroactive sites for UA and DA oxidation [31].
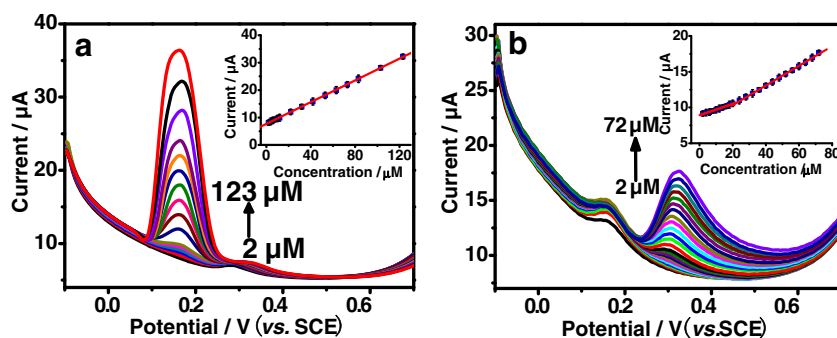
Fig. 5 DPV curves of (**a**) 2.0 mM AA, 10 μM UA, and DA at different concentrations ranging from 2.0 to 123 μM, and (**b**) 2.0 mM AA, 10 μM DA, and UA at different concentrations from 2.0 to 720 μM at pCu$_2$O NS-rGO/GCE in 0.1 M phosphate buffer (pH 7.0). Insets in A and B show the corresponding calibration curves of the oxidation peak currents against the concentrations of DA and UA, respectively. The error bars indicate the standard errors for three measurements with the same electrode

Thermogravimetric analysis (TGA) of pCu$_2$O NS-rGO was performed to investigate its thermal stability (Fig. 2A, curve a), using GO as the reference (curve b). The mass loss in weight emerged at 100, 370, and 480 °C is ascribed to the escape of interlamellar water, combustion of oxygenated functional groups, and carbon framework, respectively [32]. Compared with GO, the relatively smaller loss at 250 and 450 °C reflects the enhanced stability for pCu$_2$O NS-rGO with the metal mass loading of 33.2 %.

Figure 2B provides the Raman spectra of pCu$_2$O NS-rGO (curve a), using GO (curve b) as the reference. There are two main peaks located at 1330 and 1600 cm^{-1} for pCu$_2$O NS-rGO, corresponding to the D and G bond whose intensity ratios (denoted as I_D/I_G) are usually applied to determine the defect degree of graphitization carbon, respectively [33]. The I_D/I_G is 1.14 for pCu$_2$O NS-rGO, which is higher than that of GO (0.94), but similar to that of the previous PtNi nanoflakes/RGO (1.13) in our group [34], showing the efficient decomposition of oxygenated groups during the solvothermal synthesis.

The valence states and surface composition of the sample were characterized by X-ray photoelectron spectroscopy (XPS). As observed in survey XPS spectrum (Fig. 3a), the product mainly contains C, N, O, and Cu elements. Figure 3b depicts the oxidation state of Cu in pCu$_2$O NS-rGO. There are two main peaks located at 953.80 and 932.68 eV, which are well indexed to Cu 2p$_{1/2}$ and 2p$_{3/2}$ features of Cu^0 [35]. Besides, a weak peak at around 944 eV demonstrates the very minimal Cu^{2+} species after the reaction process [36]. It is also worth mentioned that the 2p$_{3/2}$ binding energy of Cu^0 is merely ~0.1 eV differ from Cu$^+$ [36]. Therefore, the valence state of Cu in pCu$_2$O NS-rGO is probably located between 0 and +1.

High-resolution C 1 s XPS spectra of pCu$_2$O NS-rGO (Fig. 3c) can be separated into three peaks at 284.78, 287.63, and 288.63 eV, which were indexed to the C-C (sp^2), C-O, and C = O groups, respectively [33]. The peak intensities of oxygen containing groups are much weaker than those of GO (Fig. 3d), indicating the efficient reduction of GO, as demonstrated by Raman data.

Electrochemical measurements

The electrochemical property of pCu$_2$O NS-rGO (curve a), Cu$_2$O NPs (curve b), and rGO (curve c) modified electrodes were characterized in 1.0 M KCl containing 5.0 mM [Fe(CN)$_6$]$^{3-/4-}$, using bare electrode (curve d) as the referenced. There is a couple of redox peaks presented in the respective cyclic voltammetry (CV) curves in all cases (Fig. 4A). The peak potential separation of pCu$_2$O NS-rGO (ΔE_P, 214 mV) is smaller than those of Cu$_2$O NPs (295 mV), rGO (336 mV), and bare electrode (384 mV). It reflects the faster electron transfer rate of pCu$_2$O NS-rGO, owing to the enhanced electric

conductivity of rGO. Meanwhile, the peak current (I_P) at pCu$_2$O NS-rGO/GCE (36.4 μA) is 1.23-fold, 1.26-fold, and 1.78-fold larger than those of Cu$_2$O NPs (29.6 μA), rGO (28.8 μA), and bare GCE (20.4 μA), respectively, thanks to the enlarged surface area of the unique porous structure.

The electrical conductivity of the modified electrodes was further examined by electrochemical impedance spectroscopy (EIS). Figure 4B showed the larger well-defined semicircle at higher frequencies for pCu$_2$O NS-rGO (curve a) when compared with rGO (curve b) and bare GCE (curve c) under the same conditions. It means the greatly decreased electron
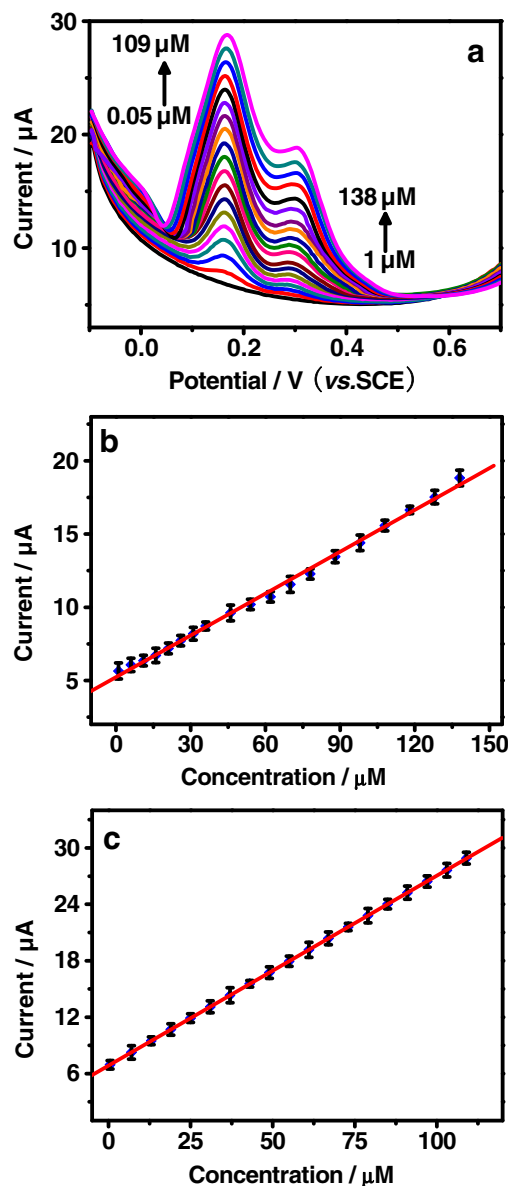
Fig. 6 **a** DPV curves at pCu$_2$O NS-rGO/GCE in 0.1 M phosphate buffer (pH 7.0) for simultaneous detection of DA and UA in the presence of 2.0 mM AA. The calibration curves of the respective oxidation peak currents against the concentrations of **b** UA (at 0.29 vs. SCE) and **c** DA (at 0.16 V vs. SCE), respectively. The error bars indicate the standard errors for three measurements with the same electrode

Table 1 Comparison with the sensors for UA and DA in the literature

Electrode materials	Linear range ($\mu mol\ L^{-1}$)		Detection limit ($\mu mol\ L^{-1}$)		Ref.
	DA	UA	DA	UA	
Poly(acrylic acid) – multiwalled carbon-nanotubes	0.04–3.0	0.3–10	0.02	0.11	[4]
Pt/rGO	10–170	10–130	0.25	0.45	[27]
Nanoporous PtCu alloy	4–20	10–70	2.8	5.7	[39]
MoS_2 /rGO	5–545	25–2745	0.05	0.46	[40]
Boron-doped multi-walled carbon nanotubes	-	-	0.11	0.65	[41]
Porous Cu_2O nanospheres-rGO	0.05–109.0	1.0–138.0	0.015	0.112	This work

transfer resistance at pCu_2O NS-rGO modified electrode. These observations were in good accordance with the CV results, indicating the efficient deposition of pCu_2O NS-rGO on the electrode surface.

Electrocatalytic behaviors of UA and DA

Fig. S1 (ESM, Electronic supplementary material) exhibits the CV curves of UA and DA at pCu_2O NS-rGO/GCE (curve b) in the presence of AA, using bare electrode (curve a) as the standard. There are two distinct oxidation peaks emerged at 407 and 260 mV (vs. SCE) for pCu_2O NS-rGO, which can be ascribed to the electrochemical oxidation of UA and DA, respectively. The ΔE_P for UA-DA is 147 mV, which would be employed for the subsequent concurrent detection of UA and DA. However, there is an overlapped oxidation peak obtained at 303 mV (vs. SCE) on the bare electrode (curve a), revealing the inefficient distinguishment of UA and DA at bare GCE.

Furthermore, the effects of the pCu_2O NS-rGO dosage (range of 4 ~ 8 μg) were investigated by CV curves for 5.0 mM $[Fe(CN)_6]^{3-/4-}$ in 1.0 M KCl solution (Fig. S2, ESM) as a redox probe by using Randles-sevcik equation [37]: $i_p = 2.69 \times 10^5 n^{3/2} ACD^{1/2} v^{1/2}$.

Where C and D are the concentration (5.0 mM) and diffusion coefficient ($7.60 \times 10^{-6}\ cm^2\ s^{-1}$) of $K_3[Fe(CN)_6]$, respectively. i_p is the anodic peak current response, n is the number of electron

transferred, v is the scan rate and A is the effective surface area. The effective surface area of pCu_2O NS-rGO increase quickly with the adding of catalyst dosage at the early stage (inset in Fig.S2, ESM), and reach relatively high level at 6 μg of pCu_2O NS-rGO. Subsequently, the effective surface area almost keeps unchanged by further increasing its dosage. Therefore, 6 μg of the catalyst was employed for the following experiments.

The pH effects in phosphate buffer (0.1 M) in the presence of 2.0 mM AA were investigated on pCu_2O NS-rGO/GCE for concurrent determination of UA and DA (Fig. S3, ESM). The I_P and ΔE_P are relatively larger at pH 7.0 as compared with the other cases, which is chosen as the optimal pH in the subsequent measurements.

DPV was devoted to simultaneously test of UA and DA at pCu_2O NS-rGO/GCE, due to its high sensitivity and selectivity [38]. Figure 5a provides the respective DPV curves at different DA concentrations in the presence of 10.0 μM UA and 2.0 mM AA. The anode peak currents toward the oxidation of DA increased linearly as the DA concentrations increase from 2.0 to 123.0 μM. The linear regression equation is $I\ (\mu A) = 7.65 + 0.20C$ ($R^2 = 0.9998$), with the detection of limit (LOD) of 48 nM. Similarly, Fig. 5b reveals that the catalytic currents increase linearly with the increased concentrations of UA from 2.0 to 720.0 μM in the presence of 10.0 μM DA and 2.0 mM AA. The regression equations are $I\ (\mu A) = 2.23 + 0.02C$ ($R^2 = 0.9902$) and $I\ (\mu A) = 1.89 +$

Fig. 7 Amperometric curves of pCu_2O NS-rGO/GCE after the addition of 2.0 mM AA, (**a**) 10.0 μM DA, (**b**) 20.0 μM UA, and other chemicals to 0.1 M phosphate buffer (pH 7.0). The applied potentials for UA and DA are 0.29 and 0.16 V (vs. SCE), respectively
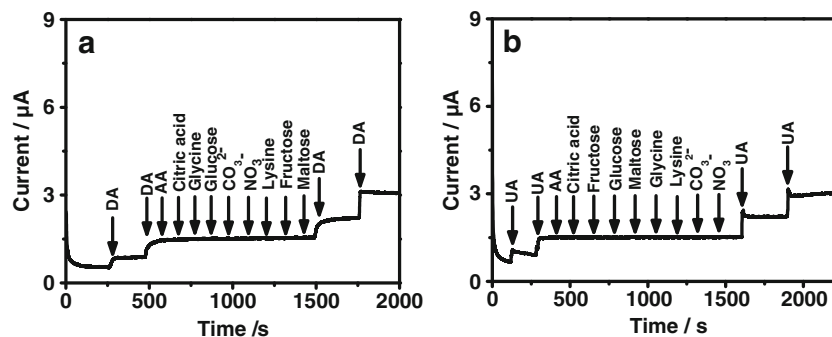
$0.03C$ ($R^2 = 0.9988$), with the LOD of 328 nM. It also indicates that there is no interference observed for the concurrent measuring of UA and DA with the existence of 2.0 mM AA.

Under the optimized experimental conditions, a series of UA and DA concentrations were simultaneously detected at pCu$_2$O NS-rGO/GCE. The electrochemical responses at 0.29 and 0.16 V (vs. SCE) are proportional to the concentrations of UA and DA, respectively (Fig. 6a), owing to the electrocatalytic oxidation of UA and DA. The linear ranges for UA and DA detection are 1.0 ~ 138.0 μM (Fig. 6b) and 0.05 to 109.0 μM (Fig. 6c), with the LOD of 112 and 15 nM (S/N = 3), respectively. These results reveal their individual or simultaneous determination with high sensitivity and selectivity in this system. Furthermore, their catalytic performances at pCu$_2$O NS-rGO/GCE are comparative to or even better than the other sensors reported previously (Table 1) [4, 27, 39–41].

The reproducibility and stability were investigated at pCu$_2$O NS-rGO/GCE for simultaneous assay of 1.0 mM UA and DA. The reproducibility was examined by using five modified electrodes prepared in the same way, and the relative standard deviation was 3.52 %. The stability was further evaluated by measuring the corresponding catalytic currents of UA and DA on the same electrode after the storage of one month in the refrigerator at 4 °C if not in use. The respective currents remained 95.1 % and 94.3 % of their initial values for UA and DA after one month, respectively. These results exhibit the excellent stability and reproducibility of the constructed sensor.

Several potential interferences were introduced to examine the anti-inference ability at pCu$_2$O NS-rGO/GCE for the electrochemical detection of 20.0 μM UA and 10.0 μM DA containing 2.0 mM AA (Fig. 7) under the optimized conditions. There was no interference detected in the presence of 100-fold citric acid, glycine, glucose, CO_3^{2-}, NO_3^-, lysine, fructose, and maltose. As a result, the sensor has potential applications for sensitive and selective detection of UA and DA in clinical samples.

Conclusions

In summary, pCu$_2$O NS-rGO was synthesized by a convenient one-pot solvothermal strategy, and employed to develop a sensor for selectively concurrent detection of UA and DA containing AA. As expected, this sensor possesses good sensitivity and selectivity, wide linear ranges, and preeminent stability in the concurrent analysis of UA and DA with the existence of 2.0 mM AA.

References

1. Zhang A, Neumeyer JL, Baldessarini RJ (2007) Recent progress in development of dopamine receptor subtype-selective agents: potential therapeutics for neurological and psychiatric disorders. Chem Rev 107:274

2. Yusoff N, Pandikumar A, Ramaraj R, Lim HN, Huang NM (2015) Gold nanoparticle based optical and electrochemical sensing of dopamine. Microchim Acta 182:2091

3. Wu L, Feng L, Ren J, Qu X (2012) Electrochemical detection of dopamine using porphyrin-functionalized graphene. Biosens Bioelectron 34:57

4. Liu A, Honma I, Zhou H (2007) Simultaneous voltammetric detection of dopamine and uric acid at their physiological level in the presence of ascorbic acid using poly(acrylic acid)-multiwalled carbon-nanotube composite-covered glassy-carbon electrode. Biosens Bioelectron 23:74

5. Zhang Y, Pan Y, Su S, Zhang L, Li S, Shao M (2007) A novel functionalized single-wall carbon nanotube modified electrode and its application in determination of dopamine and uric acid in the presence of high concentrations of ascorbic acid. Electroanalysis 19:1695

6. Zhao L, Li H, Gao S, Li M, Xu S, Li C, Guo W, Qu C, Yang B (2015) MgO nanobelt-modified graphene-tantalum wire electrode for the simultaneous determination of ascorbic acid, dopamine and uric acid. Electrochim Acta 168:191

7. Safavieh M, Ahmed MU, Tolba M, Zourob M (2012) Microfluidic electrochemical assay for rapid detection and quantification of escherichia coli. Biosens Bioelectron 31:523

8. Yang L, Liu D, Huang J, You T (2014) Simultaneous determination of dopamine, ascorbic acid and uric acid at electrochemically reduced graphene oxide modified electrode. Sens Actuators, B 193:166

9. Cai W, Lai T, Du H, Ye J (2014) Electrochemical determination of ascorbic acid, dopamine and uric acid based on an exfoliated graphite paper electrode: A high performance flexible sensor. Sens Actuators, B 193:492

10. Sanghavi BJ, Wolfbeis OS, Hirsch T, Swami NS (2014) Nanomaterial-based electrochemical sensing of neurological drugs and neurotransmitters. Microchim Acta 182:1

11. Zheng X, Zhou X, Ji X, Lin R, Lin W (2013) Simultaneous determination of ascorbic acid, dopamine and uric acid using poly(4-aminobutyric acid) modified glassy carbon electrode. Sens Actuators, B 178:359

12. Ragupathy D, Gopalan AI, Lee K-P (2010) Electrocatalytic oxidation and determination of ascorbic acid in the presence of dopamine at multiwalled carbon nanotube-silica network-gold nanoparticles based nanohybrid modified electrode. Sens Actuators, B 143:696

13. Zhang F, Li Y, Y-e G, Wang Z, Wang C (2011) One-pot solvothermal synthesis of a Cu$_2$O/graphene nanocomposite and its application in an electrochemical sensor for dopamine. Microchim Acta 173:103

14. Reddy S, Kumara Swamy BE, Jayadevappa H (2012) CuO nanoparticle sensor for the electrochemical determination of dopamine. Electrochim Acta 61:78

15. Ng CHB, Fan WY (2006) Shape evolution of Cu$_2$O nanostructures via kinetic and thermodynamic controlled growth. J Phys Chem B 110:20801

16. Hua Q, Cao T, Bao H, Jiang Z, Huang W (2013) Crystal-plane-controlled surface chemistry and catalytic performance of surfactant-free Cu$_2$O nanocrystals. ChemSusChem 6:1966

17. Liu Y, Deng Y, Sun Z, Wei J, Zheng G, Asiri AM, Khan SB, Rahman MM, Zhao D (2013) Hierarchical Cu₂S microsponges constructed from nanosheets for efficient photocatalysis. small 9: 2702

18. Zhang H, Zhu Q, Zhang Y, Wang Y, Zhao L, Yu B (2007) One-pot synthesis and hierarchical assembly of hollow Cu₂O microspheres with nanocrystals-composed porous multishell and their gas-sensing properties. Adv Funct Mater 17:2766

19. Anandan S, Wen X, Yang S (2005) Room temperature growth of CuO nanorod arrays on copper and their application as a cathode in dye-sensitized solar cells. Mater Chem Phys 93:35

20. Wang WZ, Wang G, Wang XS, Zhan Y, Liu Y, Zheng CL (2002) Synthesis and characterization of Cu₂O nanowires by a novel reduction route. Adv Mater 14:67

21. Chang Y, Teo JJ, Zeng HC (2005) Formation of colloidal CuO nanocrystallites and their spherical aggregation and reductive transformation to hollow Cu₂O nanospheres. Langmuir 21:1074

22. Park JC, Kim J, Kwon H, Song H (2009) Gram-scale synthesis of Cu₂O nanocubes and subsequent oxidation to CuO hollow nanostructures for lithium-ion battery anode materials. Adv Mater 21:803

23. Zhang L, Li H, Ni Y, Li J, Liao K, Zhao G (2009) Porous cuprous oxide microcubes for non-enzymatic amperometric hydrogen peroxide and glucose sensing. Electrochem Commun 11:812

24. Zhang L, Ni Y, Li H (2010) Addition of porous cuprous oxide to a nafion film strongly improves the performance of a nonenzymatic glucose sensor. Microchim Acta 171:103

25. Wu S, He Q, Tan C, Wang Y, Zhang H (2013) Graphene-based electrochemical sensors. Small 9:1160

26. Tang L, Wang Y, Li Y, Feng H, Lu J, Li J (2009) Preparation, structure, and electrochemical properties of reduced graphene sheet films. Adv Funct Mater 19:2782

27. Xu T-Q, Zhang Q-L, Zheng J-N, Lv Z-Y, Wei J, Wang A-J, Feng J-J (2014) Simultaneous determination of dopamine and uric acid in the presence of ascorbic acid using Pt nanoparticles supported on reduced graphene oxide. Electrochim Acta 115:109

28. Mei L-P, Song P, Feng J-J, Shen J-H, Wang W, Wang A-J, Weng X (2015) Nonenzymatic amperometric sensing of glucose using a glassy carbon electrode modified with a nanocomposite consisting of reduced graphene oxide decorated with Cu₂O nanoclusters. Microchim Acta 182:1701

29. Kuo CH, Chen CH, Huang MH (2007) Seed-mediated synthesis of monodispersed Cu₂O nanocubes with five different size ranges from 40 to 420 nm. Adv Funct Mater 17:3773

30. Shang Y, Zhang D, Guo L (2012) Cucl-intermediated construction of short-range-ordered Cu₂O mesoporous spheres with excellent adsorption performance. J Mater Chem 22:856

31. Saravanan K, Ananthanarayanan K, Balaya P (2010) Mesoporous TiO₂ with high packing density for Superior lithium storage. Energy Environ Sci 3:939

32. Pham VH, Pham HD, Dang TT, Hur SH, Kim EJ, Kong BS, Kim S, Chung JS (2012) Chemical reduction of an aqueous suspension of graphene oxide by nascent hydrogen. J Mater Chem 22:10530

33. Chen J, Sheng K, Luo P, Li C, Shi G (2012) Graphene hydrogels deposited in nickel foams for high-rate electrochemical capacitors. Adv Mater 24:4569

34. Song P, Feng J-J, Zhong S-X, Huang S-S, Chen J-R, Wang A-J (2015) Facile preparation of reduced graphene oxide supported PtNi alloyed nanosnowflakes with high catalytic activity. RSC Adv 5:35551

35. Vilar-Vidal N, Rivas J, López-Quintela MA (2012) Size dependent catalytic activity of reusable subnanometer copper(0) clusters. ACS Catal 2:1693

36. Goswami N, Giri A, Bootharaju MS, Xavier PL, Pradeep T, Pal SK (2011) Copper quantum clusters in protein matrix: potential sensor of Pb²⁺ ion. Anal Chem 83:9676

37. Madasamy T, Pandiaraj M, Balamurugan M, Bhargava K, Sethy NK, Karunakaran C (2014) Copper, zinc superoxide dismutase and nitrate reductase coimmobilized bienzymatic biosensor for the simultaneous determination of nitrite and nitrate. Biosens Bioelectron 52:209

38. Ensafi AA, Taei M, Khayamian T, Arabzadeh A (2010) Highly selective determination of ascorbic acid, dopamine, and uric acid by differential pulse voltammetry using poly(sulfonazo III) modified glassy carbon electrode. Sensors Actuators B Chem 147:213

39. Zhao D, Fan D, Wang J, Xu C (2015) Hierarchical nanoporous platinum-copper alloy for simultaneous electrochemical determination of ascorbic acid, dopamine, and uric acid. Microchim Acta 182:1345

40. Xing L, Ma Z (2015) A glassy carbon electrode modified with a nanocomposite consisting of MoS₂ and reduced graphene oxide for electrochemical simultaneous determination of ascorbic acid, dopamine, and uric acid. Microchim Acta 183:257

41. Tsierkezos NG, Ritter U, Thaha YN, Downing C, Szroeder P, Scharff P (2015) Multi-walled carbon nanotubes doped with boron as an electrode material for electrochemical studies on dopamine, uric acid, and ascorbic acid. Microchim Acta 183:35